International Journal of Material Forming (2021) 14:121–131
https://doi.org/10.1007/s12289-019-01523-1

ORIGINAL RESEARCH

Computational analysis of the extrusion process of fused deposition modeling of acrylonitrile-butadiene-styrene

Nafiseh Shadvar[1] · Ehsan Foroozmehr[1] · Mohsen Badrossamay[1] · Iman Amouhadi[1] · Alireza Shojaei Dindarloo[2]

Received: 18 April 2019 / Accepted: 25 October 2019 / Published online: 26 December 2019
© Springer-Verlag France SAS, part of Springer Nature 2019

Abstract

Die swelling is one of the paramount factors that impresses dimensional accuracy and quality of functional parts in Fused Deposition Modeling (FDM), one of the most famous Additive Manufacturing (AM) processes. Die swelling is considered a critical phenomenon in polymer extrusion process affected by melt flow rate, extruder temperature and its geometry. In this research, the ABS melt polymer behavior in the extrusion process of FDM and the die swell of extruded polymer have been investigated by empirical experiments and simulated by the Finite Element Method (FEM) using rheological properties of ABS. The internal geometry of the nozzle is investigated via analytical simulation and finite element analysis to obtain pressure and velocity distributions of the material inside the extruder as well as the die swell of extruded filament. Additionally, experiments were carried out to validate the analytical and numerical simulations. The results showed that higher melt temperature and lower material flow rate result in less pressure drop inside the nozzle and less swelling of the extruded filament.

Keywords Additive manufacturing · Fused deposition modeling · Polymer extrusion · Die swell · Rheological properties

Introduction

Fused Deposition Modeling (FDM) is one of the most well-known and widely used additive manufacturing methods in which the parts are manufactured layer by layer and based on the extrusion of polymeric filament [1]. In this process, a 3D CAD model of an intended part is transferred to the FDM machine in a form of sliced layers. In the FDM machine, a solid filamentous polymer is fed by rollers into the extruder liquefier, and transformed to the semi-molten state by a thermal coil wrapped around the liquefier. The semi-molten polymer is extruded through a nozzle by entering the solid filament, acting as a piston on it, and deposited on the substrate during the nozzle movement toward X and Y directions [2, 3]. Following the completion of the first layer, the substrate moves downward as thick as one layer toward Z axis for having a subsequent layer construction and the designed part is likewise manufactured layer by layer as it is shown in Fig. 1 [4, 5].

FDM-made parts have many applications in creating concept designs, casting patterns, and various medical, aerospace, and automotive industries [6–8]. Moreover, many composite and polymeric materials including plylactic acid (PLA), polycarbonate (PC), polycaprolactone (PCL), and acrylonitrile-butadiene-styrene (ABS) are used for part manufacturing in the FDM process [9, 10]. Among such materials, ABS is an engineering thermoplastic polymer widely used in the industry for its mechanical and processing specifications. ABS is an amorphous polymer made of three monomers: acrylonitrile, butadiene, and styrene, and it has different characteristics depending on the percentage of each monomers. Some of the unique characteristics of ABS, compared to other polymers, are its strength, impact resistance, durability, and high melting point [8, 11]. Therefore, this polymer is a suitable material to use in the FDM process for manufacturing parts in major industries, such as automotive and aerospace. The most significant parameters of the polymer extrusion process in the FDM are inlet flow rate of the filament into the extruder, the extruder temperature, and its geometry. A change in each of these parameters affects the behavior of the extruded polymeric

✉ Ehsan Foroozmehr
eforoozmehr@cc.iut.ac.ir

[1] Department of Mechanical Engineering, Isfahan University of Technology, Isfahan 8415683111, Iran

[2] Iran Polymer and Petrochemical Institute, PO Box 14965/115, Tehran, Iran

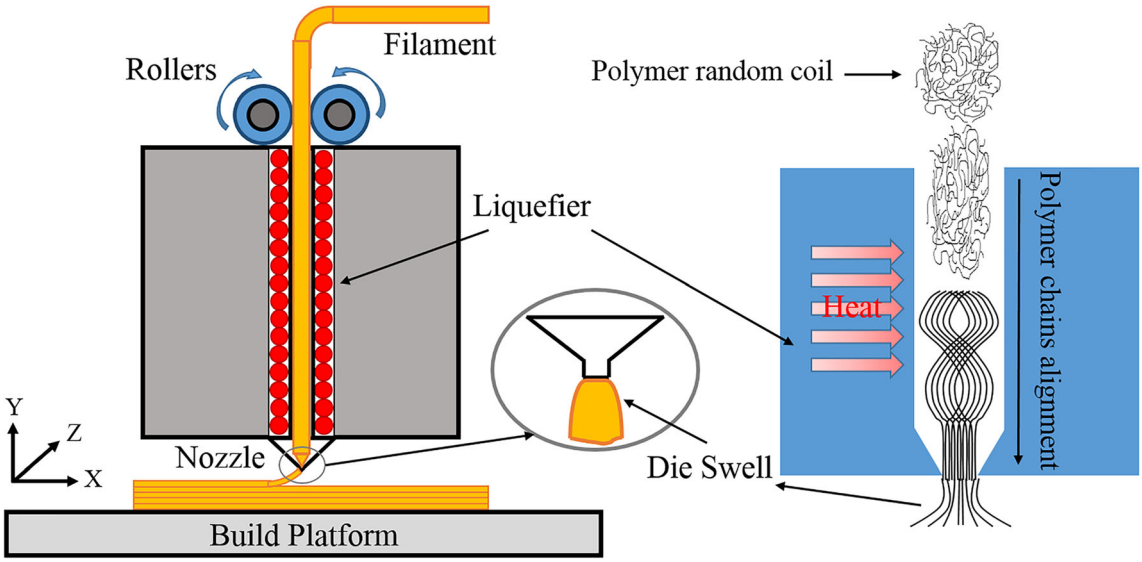

Fig. 1 The FDM machine

melt and consequently, the final part and its dimensional accuracy [12].

In the extrusion process, non-Newtonian semi-molten polymer streams in the mold. The polymeric chains are aligned with the flow direction because of shear stress formation along the die wall. These chains tend to return to their original and non-aligned state in the extruder nozzle outlet due to the elasticity of the polymer leading to an increase in diameter of the extruded polymeric raster (Fig. 1). This phenomenon is called "Die Swell", which is measured as the ratio of the extruded polymer diameter to the extruder die diameter. Die swell is one of the most important parameters determining the dimensional accuracy and the quality of production in the FDM process [13, 14].

A number of researches and analyses of the FDM process have been carried out; however, modeling of the molten polymer flow in the liquefier and nozzle outlet has not been clearly studied. Bellini modeled the FDM process for a thermoplastic filament loaded by ceramic powder. She investigated dynamics of melting region and nozzle geometry using inner extruder pressure equations and the FEM, and determined its die swell values [15]. Ramanath et al. modeled the extrusion process in the FDM for Polycaprolactone (PCL) by the FEM and analytical simulation to study the behavior of molten polymer flow and the influence of nozzle geometry variations. They concluded that the change of nozzle diameter and angle affects directly on the pressure drop along the melt flow channel [16]. Nikzad et al. carried out the finite element analysis to investigate the melt flow behavior in FDM in order to study the process ability of ABS and iron particles composite using two CFD software. Their results were shown as the profile of pressure drop, velocity and temperature along the flow channel [17]. Saadat et al. investigated the melt viscoelastic behavior and the die swell of ABS and ABS/clay nanocomposite, and their results of experiments illustrated the significant reduction in the die swell of nanocomposite samples. [18] Agrawal also examined the effect of changing nozzle geometry on the distribution of pressure drop for PCL scaffold material in the FDM process. His results showed that the reduction in nozzle diameter and angle can lead to increase pressure, which causes better resolution in fabrication. [19]. Heller et al. investigated the effects of die swell and nozzle geometry on the FDM extrusion process for a carbon fiber polymer composite using a computational approach. Their results indicated that the die swell has a large effect on the fiber orientation and the resulting mechanical properties. [13]. It seems necessary to conduct the research on the behavior of molten polymer flow in the entire FDM extrusion to determine how the process conditions of the FDM process affect die swell, which have a significant effect on the mechanical properties and dimensional accuracy of manufactured part.

In the present research, a finite element method established to investigate the die swell in a FDM extrusion process using ABS filament. The effects of inlet flow rate and extruder temperature on pressure distribution of the extruder were inspected and compared to the results of analytical simulation for validation of the results. Subsequently, the die swell rate in the nozzle outlet was modeled by FEM for the extruded polymer flow according to the viscoelastic properties of the ABS polymer. This analysis was validated by comparing the results with experimental measurements.

Materials and methods

FDM machine parameters

A FDM RapMan 3.2 machine, equipped with a direct extrusion system, is used to investigate the behavior of the ABS

polymer in the extrusion process. In this machine, rollers are placed on top of a vertical extruder for a direct feeding of the filament. The extrusion system itself consists of a liquefier with a diameter and length of 3 and 20 mm, respectively, and a nozzle with a 0.5 mm outlet diameter. The other parameters that affect the process of extrusion and manufacturing a part in the FDM machine include extruder temperature, material flow rate and extruder geometry.

Physical properties of ABS

In this study, a white ABS filament(Y&S) with 3*mm* diameter has been used. Table 1 shows the physical and thermal properties of ABS which has a glass transition temperature (T_g) at about 106 °C [20].

Variable parameters

In order to study the extrusion process of the ABS in the FDM machine, the temperature and mass flow rate of the polymer through the extruder are varied. The extruder temperature is set at three values of 220, 240 and 260 degrees Celsius. The outlet flow rate is determined by adjusting the feeding rate of the ABS filament through the extruder head using the rotary speed of its electrical motor equal to 8, 20, and 40 rpm. The equivalent volume flow rates are shown in Table 2.

FEM simulation

Flow profile of polymeric melt in the extruder can be achieved by solving simultaneously the Navier–Stokes equations: continuity (Eq. 1) and momentum (Eq. 2) [22].

$$\nabla.\overline{\nu} = 0 \tag{1}$$

$$\rho\frac{\partial\overline{\nu}}{\partial t} + \rho\overline{\nu}.\nabla.\overline{\nu} = -\nabla p + \nabla.\overline{\overline{\nu}} + \rho g \tag{2}$$

Where v refers to velocity, ρ is density, σ is stress tensor, p is hydrostatic pressure, and g is gravitational constant. This system of equations describes the governing equation of viscous flows in laminar state. In addition, energy equations shall be solved for non-isothermal flows through the flow domain. Moreover, polymeric melts classified as non-Newtonian fluids and their rheological properties are temperature dependent. By implementing suitable rheological equation for viscosity of polymer and its temperature dependency on the general flow equations, a system of equations achieves which can express flow properties in this particular domain.

In order to reduce the computational costs, with respect to the geometry and loading symmetry, an axisymmetric model is considered. In the liquefier and nozzle section, the polymer behavior is generalized toward the Newtonian state. While in the nozzle outlet region, due to the high shear stress, the polymer exhibits viscoelastic behavior [23, 24]. Thus, the finite element simulation is divided into two steps with two different non-Newtonian models for calculations.

Table 1 Physical and thermal properties of the ABS filament [20, 21]

Density ($\frac{Kg}{m^3}$)	Thermal conductivity ($\frac{W}{K.m}$)	Heat capacity ($\frac{J}{Kg.K}$)	Thermal expansion coefficient ($\frac{1}{K}$)
1200	0.2	1680	60×10^{-6}

Table 2 Volumetric flow rate of the ABS in the FDM extruder head at three motor rotational speeds

Motor rotational speed (rpm)	Measured weight of material in the outlet (g)	Calculated volume flow rate (mm^3/s)
8	0.055±0.001	0.9
20	0.125±0.004	2.1
40	0.241±0.002	4.0

Step 1

In the first step of the simulation, velocity profile and pressure distribution are investigated inside the liquefier and the extruder nozzle. A fine quadrilateral type mesh with minimum mesh size of $8.2\times10^{-3}mm$ is used. This model is used to solve motion and energy equations in a non-homogeneous and steady state flow. The two-dimensional mesh and the boundary conditions are shown in Fig. 2. The melt material enters the extruder at a fixed temperature at 200 °*C* and is conducted by the thermal flux imposed by the liquefier wall. No slip condition is imposed on the walls [22, 25].

A generalized Newtonian model is defined for the melt flow behavior. The viscosity of the molten polymer is affected by the shear rate and melt temperature [23]. Therefore, Eq. (3) is used to determine this relationship:

$$\eta = F(\dot{\gamma})\,H(T) \tag{3}$$

Where $F(\dot{\gamma})$ defines the shear rate function and $H(T)$ is the temperature function.

A capillary rheometer (Rheoscope Ceast1000) was used to obtain rheological characteristics of the ABS polymer according to ASTM D3835 [25]. This machine included a 71.63 mm^2 cross-section compartment, the capillary diameter of 1 mm, and the length of 20 mm. The test was performed at three temperature degrees of 220, 240 and 260 °C and the shear rate ranges from 10 to $1000s^{-1}$. The shear rate of the polymer melt in the capillary wall is calculated using the

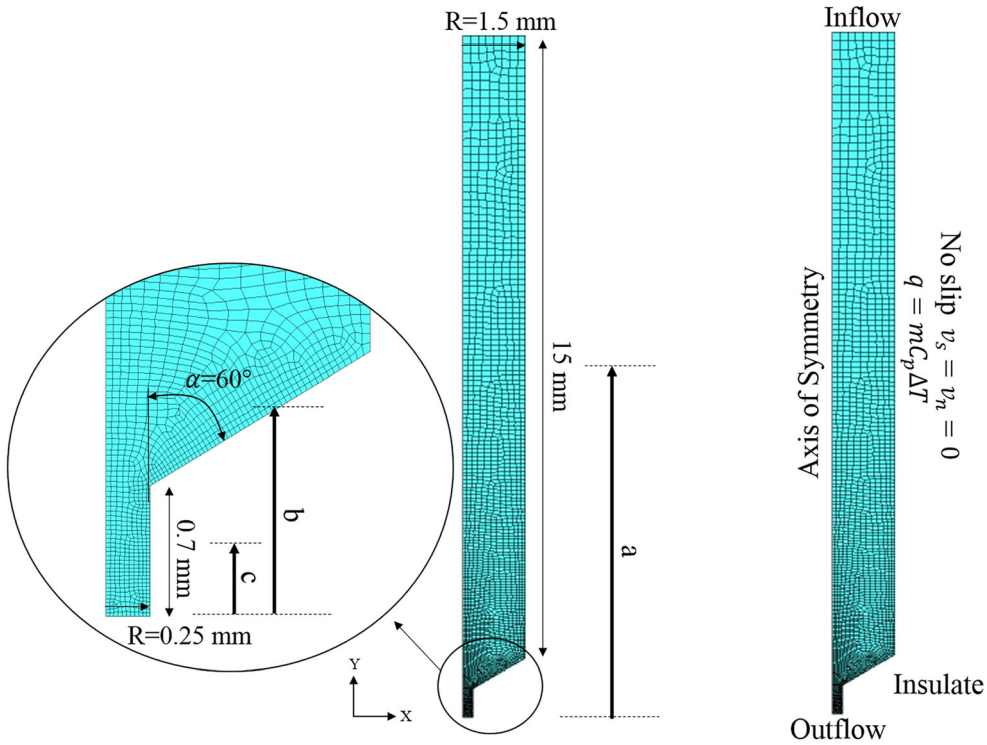

Fig. 2 Geometry, mesh, and boundary conditions of the first step

volume flow rate obtained from the piston speed and cross-sectional area, according to Eq. (4).

$$\dot{\gamma}_a = \frac{4Q}{\pi r^3} \tag{4}$$

Where $\dot{\gamma}_a$ is the shear rate, Q refers to the volume flow rate, and r is the piston radius. The wall shear stress is also obtained in accordance with the Bagley correction [25], by the difference between the atmospheric and the compartment pressure obtained from the force ratio to cross-sectional area of the compartment (Eq. 5).

$$\tau_w = \frac{r\Delta P}{2L} \tag{5}$$

Where τ_w is the wall shear stress, ΔP is the pressure difference, r is the piston radius, and L is the capillary length. The viscosity correlated to the shear rate of the polymer is equal to the ratio of wall shear stress to the shear rate (as Eq. 6).

$$\eta_a = \frac{\tau_w}{\dot{\gamma}_a} \tag{6}$$

The results regarding shear rate and viscosity are true for Newtonian fluids, while for non-Newtonian ones such as polymer melts, these values are apparent and the true shear rate and viscosity are thus to be obtained [26]. The true shear rate is obtained by the Rabinowitsch correction [25], from the apparent shear rate and the slope of the shear stress versus the apparent shear rate (Eq. 7).

$$\dot{\gamma} = \left[\frac{(3n+1)}{4n}\right]\dot{\gamma}_a \tag{7}$$

Where $\dot{\gamma}$ is the true shear rate, $\dot{\gamma}_a$ is the apparent shear rate, and n is the slope of the shear stress versus the apparent shear rate. Therefore, the true viscosity of the polymer is calculated using the wall shear stress and its true shear rate. Fig. (3) shows the logarithmic diagram of true viscosity versus true shear rate for ABS at three different temperatures.

As shown in Fig. 3, the viscosity shear rate dependency of the ABS can be expressed using power law rheological model (Eq. 8).

$$\eta = k\left(\dot{\gamma}\right)^{n-1} \tag{8}$$

Where η is the true viscosity, $\dot{\gamma}$ is the true shear rate, k is the material consistency, and n is the power law index. In Table 3 the values of n and k have been obtained from the curve fitting of rheometry data and n is the norm of residual value for curve fitting.

The viscosity-temperature dependency of the ABS is also determined using the Arrhenius equation (Eq. 9) and the diagram of true viscosity versus temperature.

$$H(\mathrm{T}) = \exp\left(\alpha\left(\frac{1}{T} - \frac{1}{T_a}\right)\right) \tag{9}$$

Where α is the activation energy and T_a is the reference temperature in which $H(\mathrm{T}) = 1$. α is obtained by measuring the

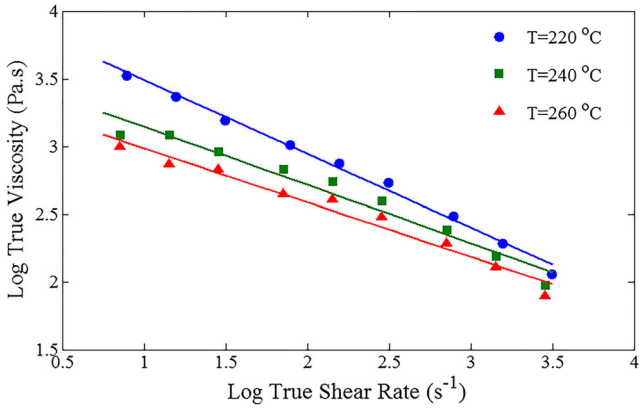

Fig. 3 Logarithmic diagram of true viscosity versus shear rate for ABS at three temperatures

slope of diagram of *log(viscosity)* vs. *invers of temperature* within the limits of the intended shear rate; therefore, α is calculated to be 3630.07 $^{1}/_{k}$ in the Arrhenius relation.

Analytical simulation of pressure

In order to validate the finite element simulation and to show the precision of its calculations, an analytical approach has been used to investigate the melt flow and pressure in the extruder. The extruder governing equations for flow and pressure has been established regarding the internal geometry of the extruder die. As it shows in Fig. 4, the extruder geometry has been divided into three zones; where zone 1 is the liquefier and zones 2 and 3 are the conical and capillary zones of the nozzle, respectively.

The governing equations has been solved using the following assumptions: laminar flow, steady state regime, incompressible flow, no-slip on the walls, and no gravity forces. Using the principle of equilibrium of mass in any element and substituting power law equation for viscosity of the ABS in the flow equation, the pressure drop can be described as follows [15, 19]:

$$\Delta P_1 = 2L_1\left(\frac{v}{\varnothing}\right)^{\frac{1}{m}}\left(\frac{m+3}{\left(D_1/2\right)^{m+1}}\right)^{\frac{1}{m}} * e^{\left(\alpha\left(\frac{1}{T}-\frac{1}{T_a}\right)\right)} \tag{10}$$

Table 3 Power law index and material consistency at various temperatures

Temperature (°C)	n	k ($Pa.\ s^n$)	n
220	0.45	10,779.53	0.11
240	0.57	3760.97	0.22
260	0.60	2434.44	0.18

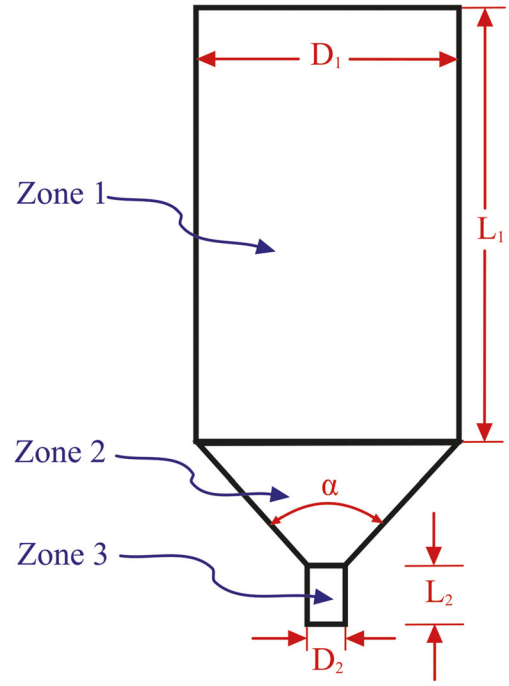

Fig. 4 Sectional view of the extruder for analytical analysis

$$\Delta P_2 = \frac{m}{3\tan\left(\alpha/2\right)}\left(\frac{v}{\varnothing}\right)^{\frac{1}{m}}\left(\frac{1}{D_2^{\frac{3}{m}}}-\frac{1}{D_1^{\frac{3}{m}}}\right) \left[\left(D_1/2\right)^2.2^{(m+3)}.(m+3)\right]^{\frac{1}{m}} * e^{\left(\alpha\left(\frac{1}{T}-\frac{1}{T_a}\right)\right)} \tag{11}$$

$$\Delta P_3 = 2L_2\left(\frac{v}{\varnothing}\right)^{\frac{1}{m}}\left(\frac{(m+3)\left(D_1/2\right)^2}{\left(D_2/2\right)^{m+3}}\right)^{\frac{1}{m}} * e^{\left(\alpha\left(\frac{1}{T}-\frac{1}{T_a}\right)\right)} \tag{12}$$

Where v is the material speed, L_1 and L_2 are the length of zones 1 and 3, D_1 and D_2 are the diameters of zones 1 and 3, and α is the angle of zone 2. Here the power law equation for viscosity is represented as $\dot{\gamma} = \varphi\tau^m$ [16, 19] associated with shear rate and shear stress. Thus, the total pressure drop can be calculated as follows:

$$\Delta P = \Delta P_1 + \Delta P_2 + \Delta P_3 \tag{13}$$

Step 2

The second step of the simulation, including the capillary of the nozzle and the extruded polymer, was carried out to investigate the die-swelling phenomenon. The two-dimensional geometry model, which is created by the quadrilateral mesh type and applied boundary conditions, are shown in Fig. 5. It is assumed that the flow rate at the inlet of the capillary is uniform with constant temperature and the semi-molten ABS polymer is incompressible. In this section, the polymeric melt on the flow temperature of 220, 240 and 260°C is extruded

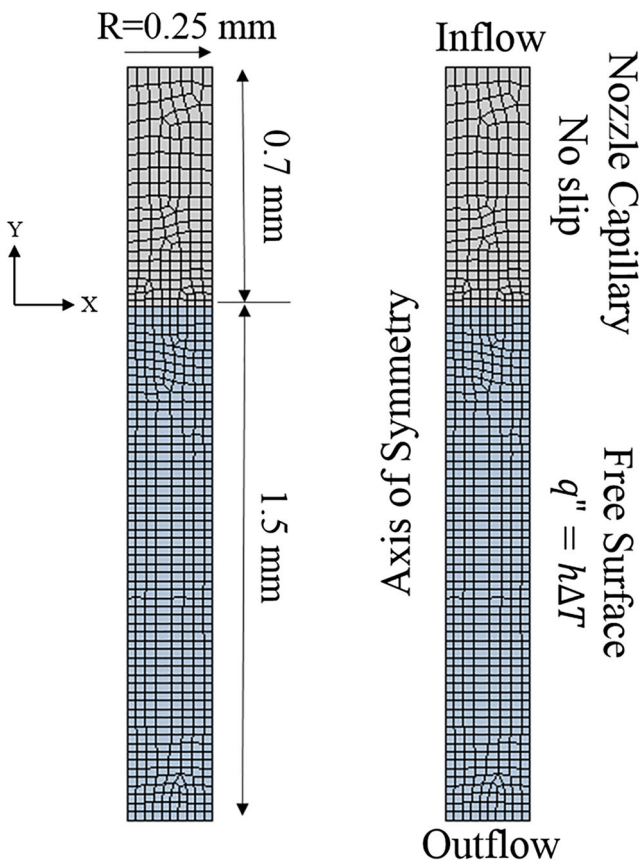

Fig. 5 Geometry, mesh and boundary conditions of the second step

from the nozzle to a free surface condition where the temperature is considered to be the room temperature.

In the capillary of nozzle, the high shear stress from the nozzle wall orients the molecular chains of the polymeric melt in the flow direction. As the material exits the die and the shear stress is removed, the long molecular chains tend to regain their original shape. The deformation is said to be in the viscoelastic range. So in the FE model, the material characteristic is considered as a linear viscoelastic model (Eq. 14). As indicated, total stress $\tau(t)$ is the sum of stresses generated at each step from t' to t, and $\dot{\gamma}$ is the shear rate. In this model, The relaxation of the molecules is described by relaxation modulus G [23].

$$\tau(t) = \int_{-\infty}^{t} G(t-t')\dot{\gamma}(t')dt' \tag{14}$$

Rheometer test used to characterize the linear viscoelastic properties of polymers involves dynamic load of the material at a strain amplitude at changing frequency. Two viscoelastic moduli: storage modulus G' and the loss modulus G'', representing the elastic and viscous part respectively, the amount of energy stored in the material and the amount of energy dissipated in the deformation, have been determined according to Eq. (14). The relation between the viscoelastic moduli and angular frequency(ω) can be expressed as complex viscosity(η^*) consisting of the viscous and elastic parts (Eq. 15).

$$|\eta^*| = \sqrt{\left(\eta'^2 + \eta''^2\right)} = \sqrt{\left[\left(\frac{G'}{\omega}\right)^2 + \left(\frac{G''}{\omega}\right)^2\right]} = \frac{|G^*|}{\omega} \tag{15}$$

The viscoelastic parameters of ABS were obtained by Saadat et al. using Rheometric mechanical spectrometer with parallel plate system [18].

Results and discussions

Temperature, velocity, and pressure distribution in the extruder

The temperature distribution of the ABS in the extruder channel is depicted in Fig. 6 for the flow rate of $2.1\frac{mm^3}{s}$. As indicated, the material temperature reaches $260°C$ by traveling about 30% of the liquefier. For comparing the material behavior in other flow rates, the temperature distribution versus central axial along the extruder die is shown in Fig. 7 for three flow rates. For flow rate of $0.9\frac{mm^3}{s}$, the melt ABS temperature reaches $260°C$ at about $10mm$ before outlet. However, for flow rate of $4.0\frac{mm^3}{s}$ it happens at about $2mm$ before outlet.

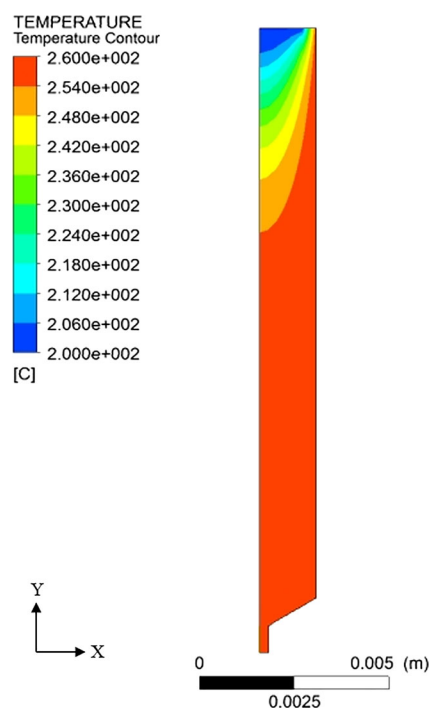

Fig. 6 The ABS temperature distribution in the molten stream channel for the flow rate of $2.1\ \frac{mm^3}{s}$; FEM

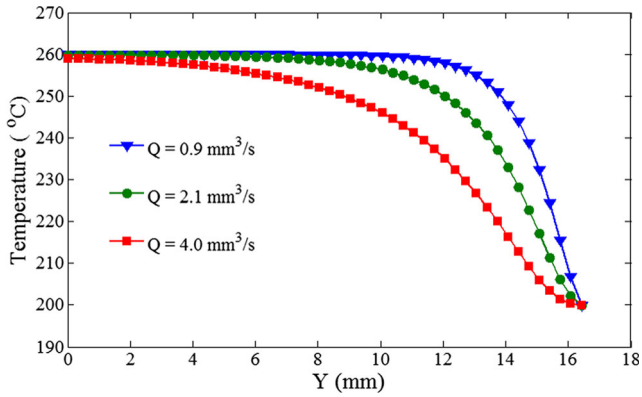

Fig. 7 Temperature distribution versus central axial along the extruder die for three flow rates, FEM

The same behavior of melt is repeated for temperatures at 220 and 240°C.

The extruder pressure distribution for the inlet flow rates of 0.9, 2.1, and 4.0 $\frac{mm^3}{s}$ and different temperature degrees at 220, 240, and 260 $°C$ are calculated. Fig. 8a, b demonstrates the contour of pressure distribution of the molten ABS in the extruder for flow rate of 2.1$\frac{mm^3}{s}$ at 260°C. According to Fig. 8a, b, the highest pressure is found to be in the stream at the liquefier equal to $2.051 \times 10^5 Pa$. The pressure is dropped rapidly by approaching the outlet.

The results of pressure distribution along the central axial of the extruder are presented in Fig. 9 for three flow rates at temperature of 260°C. As indicated, as well as for other temperatures at 220 and 240°C, three diagram have the same trend at the liquefier and in the nozzle outlet, all of them decrease to zero. For supporting this results by analytical simulation, according to the equation of continuity (Eq. 1) and momentum (Eq. 2), the pressure is dropped by the reduction of the channel diameter as a sequence of velocity increase in the smaller cross sections.

To investigate the temperature effects on pressure distribution, Fig. 10 shows the extruder maximum pressure versus temperature in various flow rates for the finite element simulation and analytical simulation. As indicated in Fig. 3, the viscosity decreases by increasing the temperature, and therefore, less pressure is expected by increasing the temperature. In Fig. 10, the similar trend is reported for both analytical and FE simulations. However, there is average of 10% difference between their values. This can be explained by the fact that the analytical model contains simplifications for pressure equations as well as lack of longitudinal stream velocity. Similar observations have been reported by Ramanath et al. [16] and Mostafa et al. [18].

As Fig. 11a, b shows, the velocity contours of the semi-molten ABS stream in the FDM extruder for the flow rate of 2.1 $\frac{mm^3}{s}$ and temperature at 260°C, the stream velocity is uniform and constant in the longer length of the liquefier. However, as indicated in velocity diagram on three lines, a,

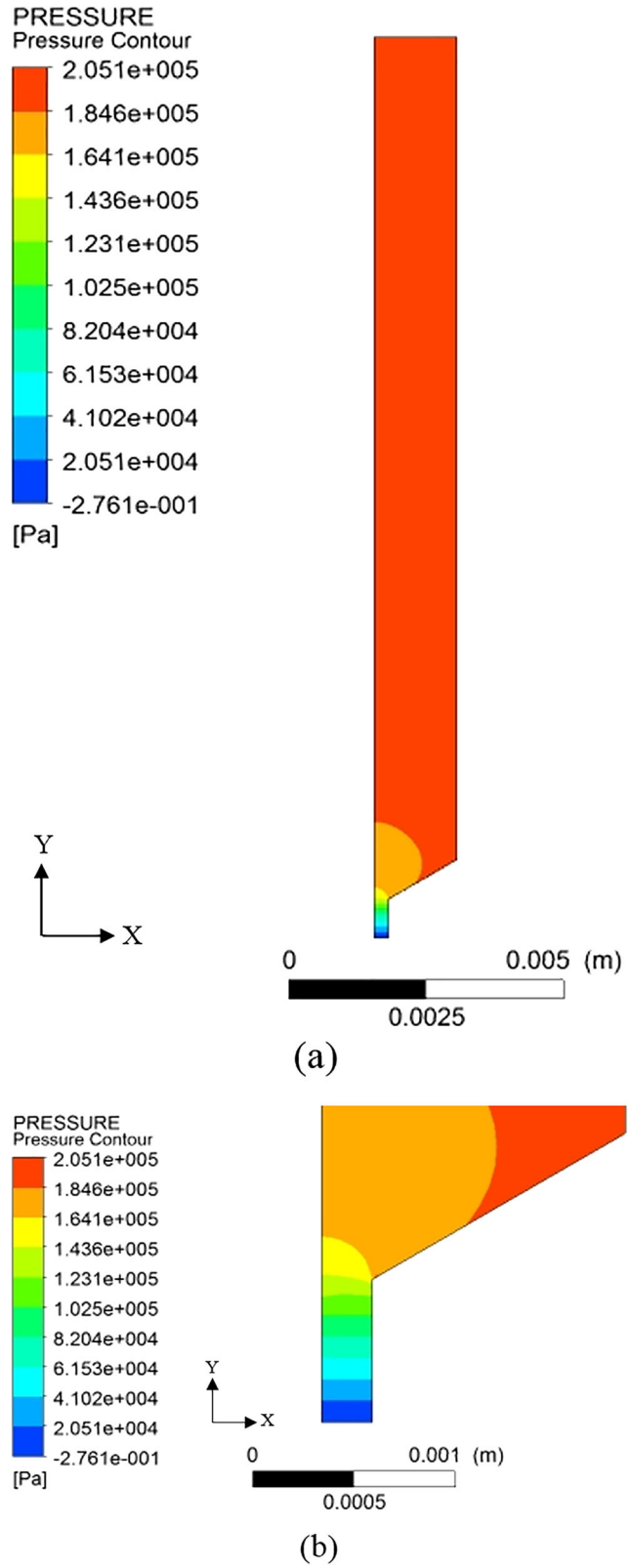

Fig. 8 **a**, **b** Pressure distribution of the ABS for flow rate of 2.1 $\frac{mm^3}{s}$ and temperature at 260 °C; FEM

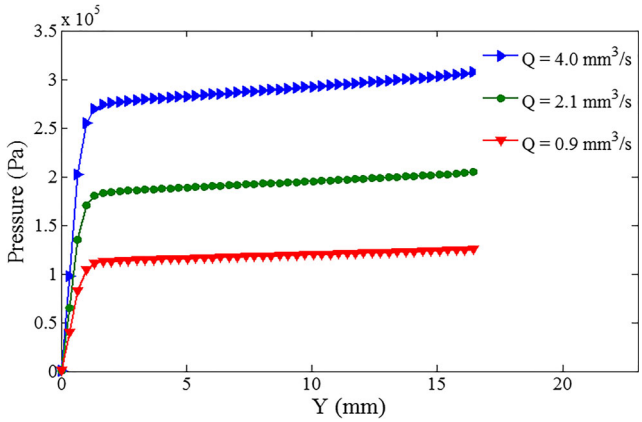

Fig. 9 Pressure distribution along the central axial for temperature at 260 °C

b and c (Fig. 2) in the extruder channel in Fig. 12, the velocity increases in the conical region of the nozzle and capillary part due to the decrease of cross section area. Therefore, the wall shear stress increases significantly and reaches its maximum value before leaving the nozzle. The higher shear stress leads to higher polymer chains alignment, which affects the die swell the most. Therefore, it is critical to calculate the velocity and shear rate values in narrow part of the nozzle. In the next section, this phenomenon is investigated.

Die swell of the extruded polymer

As the result of second section of simulation, the shear rate distribution in the capillary region of the nozzle and the die swell phenomenon at its outlet is shown in Fig. 13 for the extruder temperature of 260 °C and flow rate of 2.1 $\frac{mm^3}{s}$. As well as, the diagram of Shear rate versus X axial for three distance of Y axial is depicted in Fig. 14. As indicated, the shear rate in the capillary($Y = 0.35mm$) increases near the capillary wall due to the no-slip condition and it has highest value at the nozzle outlet($Y = 0.0mm$). As the polymer melt is extruded out from the nozzle outlet, the shear rate reduces

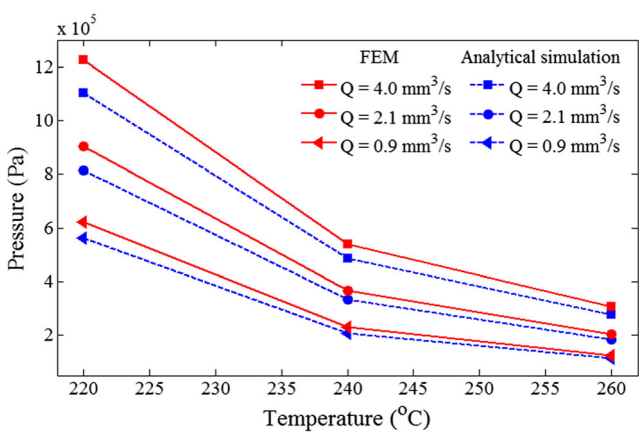

Fig. 10 Pressure diagram versus temperature in various flow rates for FEM and analytical simulation

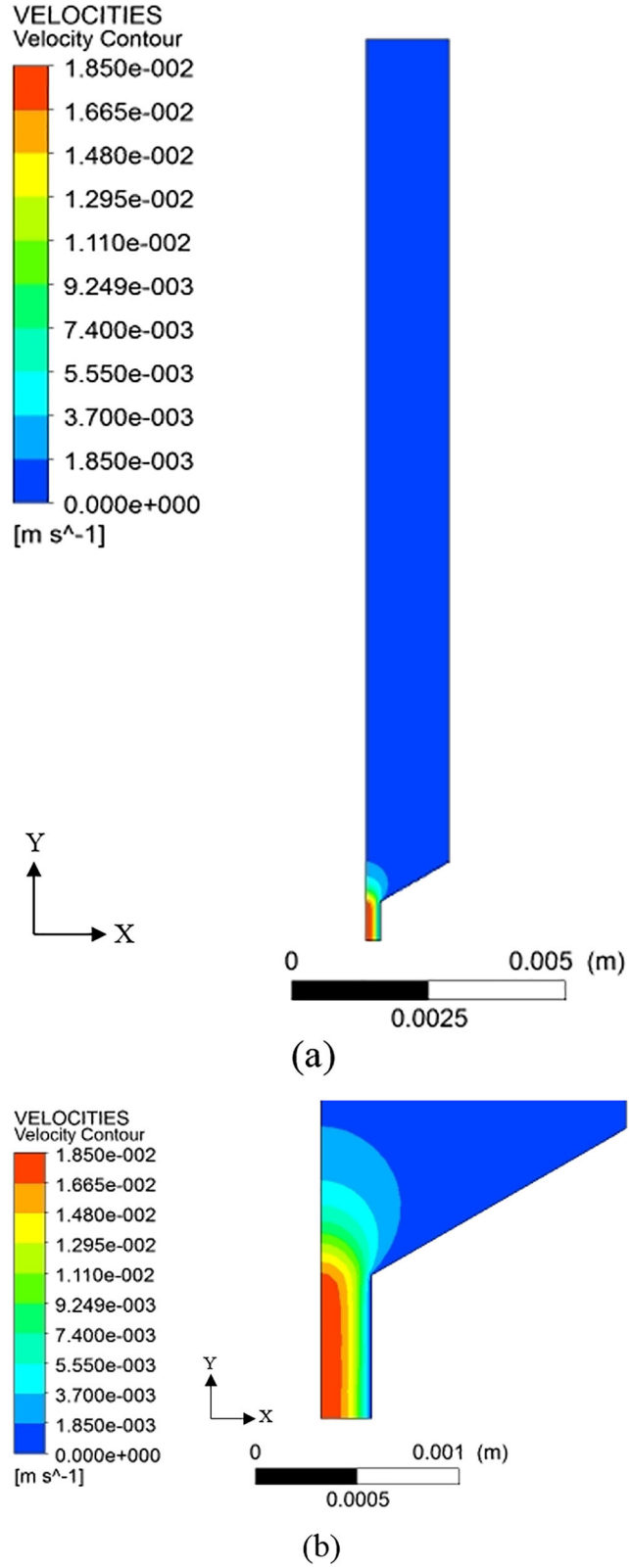

Fig. 11 **a**, **b**: Velocity distribution of the ABS for flow rate of 2.1 $\frac{mm^3}{s}$ and temperature at 260 °C

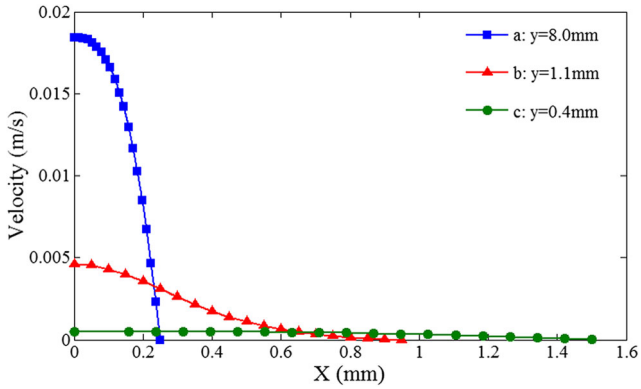

Fig. 12 Velocity diagram versus X axial on three line in extruder channel at 2.1$\frac{mm^3}{s}$ and 260°C

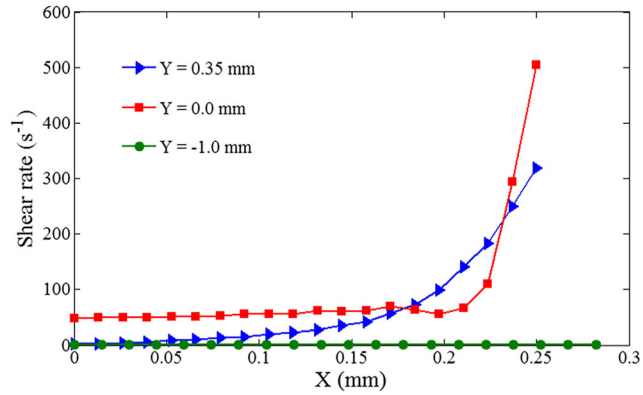

Fig. 14 Shear rate diagram versus X axial for three lengths at 260 °C and 2.1 $\frac{mm^3}{s}$

rapidly and as shown, in $Y = -1.0mm$ the shear rate is almost zero.

Die swell rate is defined as the ratio of the extruded polymer diameter to the inner capillary diameter. In the experimental study of the die swell phenomenon, the ABS polymer samples were extruded from the FDM device at different temperatures and flow rates associated with the finite element simulations. Then, these polymer samples were quickly quenched and the diameter of each sample was measured using Jenius optical microscope.

The results of die swell based on temperature in three flow rates for the experimental test and finite element simulation is shown in Fig. 15. This diagram displays similar trend of die swell analysis using the finite element model in different temperatures for a specified flow rate compared to the experimental test. In both cases, die swell rate of ABS polymer decreases almost linearly by increasing the temperature and increases by increasing the material flow rate. When the temperature of the melt is increased, the Brownian motions of polymer chains augment and the free volume around them increases. It causes easier flow and decreased viscosity, and allows molecules to slide easier among each other [23, 27, 28]. As a result, stress relaxation occurs and the retrieval of the performed modification in the stream is reduced. When the temperature is constant; despite the increase in flow rate and subsequently melt velocity in the liquefier, shear stress increases in the nozzle and leads to increase elastic energy conserved in the semi-molten ABS. Thus, when polymer is extruded from the die, die swell increases synchronously along with elastic recovery of molecular chains [23].

However, a difference of about 20% is observed between the two experimental and simulation diagrams. This difference is due to the temperature fluctuations, quenching process, or simplifications and assumptions in the finite element simulation such as the uniform velocity and temperature at the

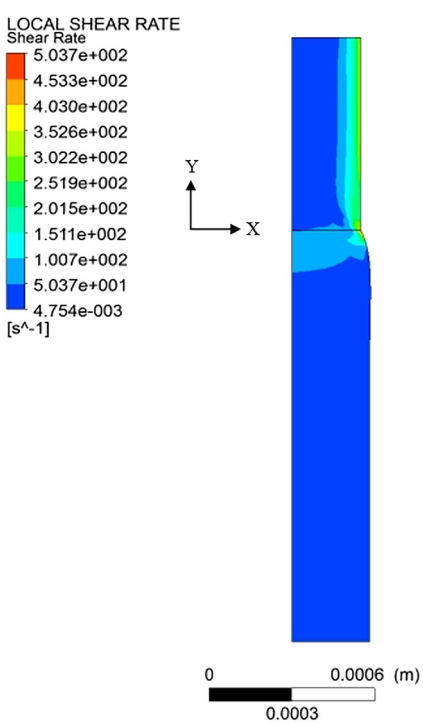

Fig. 13 Shear rate distribution in the nozzle capillary and die swell at the nozzle outlet at 260 °C and 2.1 $\frac{mm^3}{s}$

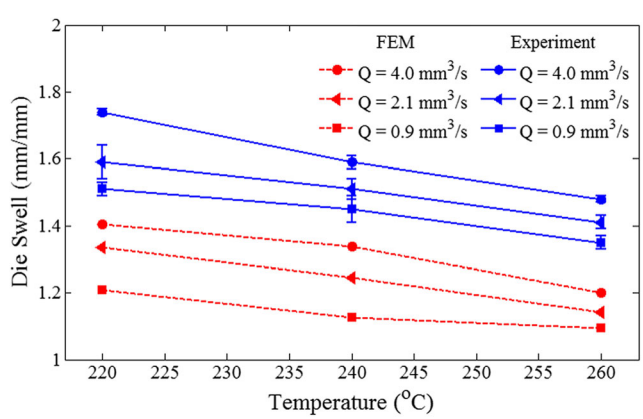

Fig. 15 Diagram of die swell versus temperature at various flow rate for experiment and FEM

inlet. Therefore, regarding the results of the die swell obtained from experimental test, the simulation of the finite element can be justifiable and the experimental results validates the simulation results.

Regarding the die swell results obtained from the experimental and finite element analysis of the ABS polymer, some suggestions have been proposed for the purpose of controlling the die swell which has a significant role in dimensional accuracy of manufactured parts by the FDM device. Obviously, the die swell lies in minimum level by setting the machine on the highest temperature and lowest flow rate. However, considering the economic aspects of using FDM, the flow rate can be considered to a higher value, and in parallel, the effect of swelling on the extruded material is adjusted in the FDM software so that the overall dimension remains precise. For the FDM RapMan system, the extruder temperature and flow rate can be set as 260 °C and 2.1 $\frac{mm^3}{s}$, respectively.

Conclusions

In this research, the behavior of the ABS thermoplastic polymer in the extrusion process of the FDM additive manufacturing procedure was analyzed. The objective was to investigate pressure distribution inside the extruder zone and die swell of the extruded polymer, which played a considerable role in determining quality and dimensional accuracy of manufactured polymer parts. For this purpose, the extrusion process was simulated in two stages applying the finite element procedure using the Ansys-Polyflow software.

Various entry flow rates (0.9, 2.1 and 4.0 $\frac{mm^3}{s}$) and extruder temperature (220, 240 and 260 °C) were studied as main effective parameters. Rheological properties of the ABS polymer were obtained using the capillary rheometry test in the form of Power Law and Arrhenius models for viscosity dependency on the shear rate and temperature, respectively. Based on the ABS polymer properties, pressure distribution inside the extruder was studied using the finite element simulation and analytical calculations. The results revealed that by the increase of the flow rate, pressure drop of the extruder increased and by the decrease of the temperature, pressure drop decreased. In the second section of simulation, the die swell rate of the ABS in the nozzle outlet of extruder was obtained using viscoelastic properties of the ABS polymer and likewise it was compared to the results obtained from the experimental measurements of die swell. Die swell studies showed that by the increase of the flow rate, the die swell increased and by the increase of the extruder temperature, this value decreased. Therefore, the results of this investigation can be used to improve the quality and dimensional precision of polymeric manufactured parts through the FDM additive manufacturing.

Compliance with ethical standards

Conflict of interest The authors declare that they have no conflict of interest.

References

1. Horta J, Simões F, Mateus A (2017) Large scale additive manufacturing of eco-composites. International Journal of Material Forming:1–6
2. Ryder MA, Lados DA, Iannacchione GS, Peterson AM (2018) Fabrication and properties of novel polymer-metal composites using fused deposition modeling. Compos Sci Technol 158:43–50
3. Bikas H, Stavropoulos P, Chryssolouris G (2016) Additive manufacturing methods and modelling approaches: a critical review. Int J Adv Manuf Technol 83(1–4):389–405
4. Garg A, Bhattacharya A, Batish A (2016) On surface finish and dimensional accuracy of FDM parts after cold vapor treatment. Mater Manuf Process 31(4):522–529
5. Grimmelsmann N, Kreuziger M, Korger M, Meissner H, Ehrmann A (2018) Adhesion of 3D printed material on textile substrates. Rapid Prototyp J 24(1):166–170
6. Carneiro O, Silva A, Gomes R (2015) Fused deposition modeling with polypropylene. Mater Des 83:768–776
7. Aliheidari N, Tripuraneni R, Ameli A, Nadimpalli S (2017) Fracture resistance measurement of fused deposition modeling 3D printed polymers. Polym Test 60:94–101
8. Uddin M, Sidek M, Faizal M, Ghomashchi R, Pramanik A (2017) Evaluating mechanical properties and failure mechanisms of fused deposition modeling acrylonitrile butadiene styrene parts. J Manuf Sci Eng 139(8):081018
9. Novakova-Marcincinova L (2012) Application of fused deposition modeling technology in 3D printing rapid prototyping area. Manuf Ind Eng 11(4):35–37
10. Gaal G, Mendes M, de Almeida TP, Piazzetta MH, Gobbi ÂL, Riul A Jr, Rodrigues V (2017) Simplified fabrication of integrated microfluidic devices using fused deposition modeling 3D printing. Sensors Actuators B Chem 242:35–40
11. Elgeti SN (2011) Free-surface flows in shape optimization of extrusion dies. RWTH Aachen University
12. Domingo-Espin M, Puigoriol-Forcada JM, Garcia-Granada A-A, Lluma J, Borros S, Reyes G (2015) Mechanical property characterization and simulation of fused deposition modeling polycarbonate parts. Mater Des 83:670–677
13. Heller BP, Smith DE, Jack DA (2016) Effects of extrudate swell and nozzle geometry on fiber orientation in fused filament fabrication nozzle flow. Addit Manuf 12:252–264
14. Mu Y, Hang L, Chen A, Zhao G, Xu D (2017) Influence of die geometric structure on flow balance in complex hollow plastic profile extrusion. Int J Adv Manuf Technol 91(1–4):1275–1287
15. Bellini A (2002) Fused deposition of ceramics: a comprehensive experimental, analytical and computational study of material behavior, fabrication process and equipment design. Drexel University
16. Ramanath H, Chua C, Leong K, Shah K (2008) Melt flow behaviour of poly-ε-caprolactone in fused deposition modelling. J Mater Sci Mater Med 19(7):2541–2550

17. Mostafa N, Syed HM, Igor S, Andrew G (2009) A study of melt flow analysis of an ABS-Iron composite in fused deposition modelling process. Tsinghua Science & Technology 14:29–37
18. Saadat A, Nazockdast H, Sepehr F, Mehranpour M (2010) Linear and nonlinear melt rheology and extrudate swell of acrylonitrile-butadiene-styrene and organoclay-filled acrylonitrile-butadiene-styrene nanocomposite. Polym Eng Sci 50(12):2340–2349
19. Agrawal A (2014) Computational and mathematical analysis of dynamics of fused deposition modelling based rapid prototyping technique for scaffold fabrication
20. Tadmor Z, Gogos CG (2013) Principles of polymer processing. Wiley, Hoboken
21. Zhang Y, Chou Y (2006) Three-dimensional finite element analysis simulations of the fused deposition modelling process. Proc Inst Mech Eng B J Eng Manuf 220(10):1663–1671
22. Nassehi V (2002) Practical aspects of finite element modelling of polymer processing. Wiley, Chichester
23. Aho J (2011) Rheological characterization of polymer melts in shear and extension: measurement reliability and data for practical processing
24. Tingting Z, Guoning R, Jinhua P (2014) Numerical simulation of three dimensional flow fields for extrusion process of GR-35 double-base propellant. Proc Eng 84:920–926
25. 02 D (2003) Standard test method for determination of properties of polymeric materials by means of a capillary Rheometer. ASTM Standards
26. Kaseem M, Hamad K (2016) Capillary flow behavior of polycarbonate (PC)/acrylonitrile–butadiene–styrene (ABS) blends. J Composit Biodegrad Polym 4:11–15
27. Ariff ZM, Ariffin A, Jikan SS, Rahim NAA (2012) Rheological behaviour of polypropylene through extrusion and capillary rheometry. In. InTech, Rijeka
28. Liang JZ (2002) Effects of extrusion conditions on rheological behavior of acrylonitrile–butadiene–styrene terpolymer melt. J Appl Polym Sci 85(3):606–611

Publisher's note Springer Nature remains neutral with regard to jurisdictional claims in published maps and institutional affiliations.